Interaction of adult human neural crest-derived stem cells with a nanoporous titanium surface is sufficient to induce their osteogenic differentiation

Stem Cell Research (2014) 13, 98–110

Available online at www.sciencedirect.com

ScienceDirect

www.elsevier.com/locate/scr

Interaction of adult human neural crest-derived stem cells with a nanoporous titanium surface is sufficient to induce their osteogenic differentiation

Matthias Schürmann[a], Annalena Wolff[b], Darius Widera[a], Stefan Hauser[c], Peter Heimann[a], Andreas Hütten[b], Christian Kaltschmidt[a], Barbara Kaltschmidt[c,*]

[a] Department of Cell Biology, Faculty of Biology, University of Bielefeld, 33615 Bielefeld, Germany
[b] Thin Films & Physics of Nanostructures, Faculty of Physics, University of Bielefeld, 33615 Bielefeld, Germany
[c] Molecular Neurobiology, Faculty of Biology, University of Bielefeld, 33615 Bielefeld, Germany

Received 18 December 2013; received in revised form 28 April 2014; accepted 29 April 2014

Abstract Osteogenic differentiation of various adult stem cell populations such as neural crest-derived stem cells is of great interest in the context of bone regeneration. Ideally, exogenous differentiation should mimic an endogenous differentiation process, which is partly mediated by topological cues. To elucidate the osteoinductive potential of porous substrates with different pore diameters (30 nm, 100 nm), human neural crest-derived stem cells isolated from the inferior nasal turbinate were cultivated on the surface of nanoporous titanium covered membranes without additional chemical or biological osteoinductive cues. As controls, flat titanium without any topological features and osteogenic medium was used. Cultivation of human neural crest-derived stem cells on 30 nm pores resulted in osteogenic differentiation as demonstrated by alkaline phosphatase activity after seven days as well as by calcium deposition after 3 weeks of cultivation. In contrast, cultivation on flat titanium and on membranes equipped with 100 nm pores was not sufficient to induce osteogenic differentiation. Moreover, we demonstrate an increase of osteogenic transcripts including Osterix, Osteocalcin and up-regulation of Integrin β1 and α2 in the 30 nm pore approach only. Thus, transplantation of stem cells pre-cultivated on nanostructured implants might improve the clinical outcome by support of the graft adherence and acceleration of the regeneration process.

Abbreviations: NCSCs, neural crest-derived stem cells; MSCs, mesenchymal stem cells; FGF-2, fibroblast growth factor-2; EGF, epidermal growth factor; ITSCs, inferior turbinate stem cells; RT, room temperature; PFA, paraformaldehyde; qRT-PCR, quantitative reverse transcription polymerase chain reaction; SEM, scanning electron microscope; ALP, alkaline phosphatase; ddH_2O, double distilled water; FCS, fetal calf serum; PBS, phosphate buffered saline; DAI, days after induction; FAK, Focal-Adhesion-Kinase.

* Corresponding author at: Molecular Neurobiology, University of Bielefeld, Universitätsstr. 25, D-33615 Bielefeld, Germany.
E-mail address: barbara.kaltschmidt@uni-bielefeld.de (B. Kaltschmidt).

http://dx.doi.org/10.1016/j.scr.2014.04.017

Introduction

Cranial neural crest-derived stem cells (NCSCs) represent an adult dormant stem cell population able to give rise to ectodermal and mesenchymal derivatives (reviewed in (Kaltschmidt et al., 2012)). It should be mentioned, that in the head region bones are generated by neural crest cells. We and others demonstrated *in vitro* an efficient mesodermal differentiation of NCSCs derived from different craniofacial regions making this cell population a promising candidate for future use in regenerative medicine (Widera et al., 2009) (Delorme et al., 2010; Dong et al., 2010; Hauser et al., 2012; Kawanabe et al., 2010; Marynka-Kalmani et al., 2010). Especially in context of bone regeneration under contribution of autologously transplanted stem cells, directed differentiation of human NCSCs into an osteogenic lineage has gained great interest. Usually, the *in vitro*-osteogenesis by cranial NCSCs is induced by supplementation of the cultivation medium with a cocktail of (bio-) chemical agents including the synthetic glucocorticoid dexamethasone (Baek et al., 2013; Calloni et al., 2009). Importantly, *in vivo*, dexamethasone exhibits severe side effects common to other glucocorticoids including immunosuppressant action, which could increase the risk of infection after autologous transplantation of NCSCs. Moreover, dexamethasone was reported to transform human NCSCs into tumorigenic phenotype in the SCID mice transplantation model (Marynka-Kalmani et al., 2010). Thus, osteogenic differentiation protocols for future clinical use ideally should avoid harsh chemical cues.

Since physiological differentiation of neural crest cells towards osteogenic lineage is at least partly mediated by the topology (e.g. the porous surface of the present bone) (Dangaria et al., 2011), the use of physical and topological cues as an osteogenic trigger has gained great interest. Indeed appropriate nanoscale topology has been reported to induce osteogenic differentiation of a variety of cell types including osteogenic cell lines, immature human osteoblasts and mesenchymal stem cells (MSCs) (Dalby et al., 2006, 2007; Lavenus et al., 2011). However, to our knowledge, there are no reports on topological induction of osteogenic differentiation for multipotent human NCSCs.

In the last couple of years several craniofacial NCSC-populations within the head were described. Such cells were identified e.g. within the dental pulp and the periodontal ligament (Arnold et al., 2010; Waddington et al., 2009; Widera et al., 2007). Importantly, adult stem cells tend to transform towards tumorigenic phenotype during long-term *in vitro* expansion (Kaus et al., 2010; Nguyen et al., 2013). Thus, due to the limited source material dental pulp-derived and periodontal stem cells are not ideal candidates for up-scaling and their future clinical use. Noteworthy, as recommended by the Food and Drug Administration (FDA), the cultivation time of human stem cells for transplantation purposes should not exceed five weeks (Fink, 2009). NCSCs derived from the human inferior turbinate (inferior turbinate stem cells / ITSCs) have the advantage of easy accessibility and relatively high frequency within the tissue of origin. Moreover, large amounts of inferior turbinate tissue are routinely removed during surgeries against snoring without severe side effects (Fairbanks, 1985). In a previous study, we demonstrated that human inferior turbinates contain 16.55 + 5.1% p75 expressing ITSCs independent from the age and the gender of the donor (Hauser et al., 2012). In addition, ITSCs could be efficiently cultivated and rapidly expanded in a FCS-free medium in a closed cGMP-grade cell culture system without changing their stemness characteristics (Greiner et al., 2011, 2014).

Titanium is a common and broadly used material in orthopedic devices (reviewed in (Wennerberg and Albrektsson, 2009)). Besides its well-known biocompatibility, it has mechanical properties similar to bone, making titanium an ideal candidate for the design of stem cell-supported prostheses, which may improve the osseointegration into the surrounding bone. Moreover, titanium surfaces can be topographically manipulated at the nanometer scale, thereby improving their biocompatibility and potential to integrate into the bone (for review see (Lavenus, Ricquier, Louarn and Layrolle, 2010; Sjostrom et al., 2013; Wennerberg and Albrektsson, 2009). Indeed Lavenus et al. reported in 2011 that nanofeatured titanium surfaces are well biocompatible and induce osteogenic differentiation of human MSCs (Lavenus et al., 2011).

In this study, we investigated the biocompatibility and influence of anisotropically arranged nanopores with 30 nm and 100 nm diameter on human neural crest-derived ITSCs. Polycarbonate membranes with 30 nm as well as 100 nm nanopores were covered with a 5 nm titanium layer and used in cell culture as a substrate. Here, we demonstrate that a nanoporous titanium surface is biocompatible with adult ITSCs. We further show that a titanium surface with a pore size of 30 nm and not of 100 nm is able to induce osteogenic differentiation of ITSCs without biochemical cues, as demonstrated by alkaline phosphatase (ALP) activity and calcium depositions visualized using Alizarin Red S and von Kossa staining. Moreover, using qRT-PCR, we demonstrate a significantly elevated transcript level for osteogenic marker genes including Osterix and Osteonectin in ITSCs cultivated on titanium with 30 nm pores compared to flat titanium and titanium surface with a 100 nm pore size. Future studies will investigate the potential replacement of FSC as a component of the differentiation medium by human blood plasma, which can be applied autologously and supports growth of ITSCs without affecting their stem cell characteristics (Greiner et al., 2011, 2014).

In sum, we show that titanium is highly biocompatible with adult human NCSCs and that nanofeaturing of such a surface with anisotropic 30 nm pores is sufficient to induce their osteogenic differentiation.

Materials and methods

Generation of a nanoporous titanium surface

To make the substrates suitable for further experiments single discs with diameters of 10 mm and 20 mm were blanked out of the track etched polycarbonate membrane (Whatman). Following this the discs and the flat glass control substrate were washed with 100% EtOH, sputtered with a 5 nm titanium layer, washed with ddH_2O, affixed in 12 well cell culture plate (TPP) and sterilized with UV irradiation.

Isolation and cultivation of neural crest-derived human ITSCs

Human inferior turbinates were obtained by biopsy during a routine surgery after an informed consent according to local (Bezirksregierung Detmold/Münster) and international guidelines. Cell isolation and cultivation were performed as described in Hauser et al. (2012). Briefly, inferior turbinates were mechanically and enzymatically dissociated and further cultivated in a serum-free medium (DMEM/F12 containing B27 supplement, FGF-2 and EGF). For rapid expansion ITSCs were cultivated in a medium supplemented with 10% human blood plasma as described in Greiner et al. (2011).

Immunocytochemistry and staining for F-actin

For nestin detection, cultivated neurospheres were seeded for 30 min on poly-D-lysin coated Lab-Tek II chambers and fixed in phosphate buffered 4% paraformaldehyde (PFA, Sigma-Aldrich) for 20 min at RT. Cells were permeabilized for 30 min with 0.02% Triton X-100 followed by incubation with primary antibodies against nestin (mouse anti-nestin 1:100 (Millipore)). Secondary fluorochrome-conjugated antibodies were diluted 1:300 (goat anti-mouse Alexa 555; Molecular Probes) and incubated for 1 h at RT followed by nuclear counterstaining with SYTOX green (1:2000, Molecular Probes). Fluorescence imaging was performed using confocal microscopy (LSM 510, Carl Zeiss).

For immunocytochemical detection of phosphorylated FAK or F-actin, ITSCs were fixed after 1 day of cultivation using 100% methanol for 5 min at −20 °C or 4% PFA at RT for 20 min. Subsequently the cells were treated with 1% BSA, 10% goat serum, 0.3 M glycin and 0.1% Tween 20 (Amresco) in 1 × PBS for 1 h at RT. Following this the cells were incubated with either a primary antibody against Focal-Adhesion-Kinase (FAK) phosphorylated at Y397 (ab 81298 1:100) overnight at 4 °C or rhodamine coupled phalloidin (1:150, Sigma-Aldrich) in PBS for 1 h at RT followed by nuclear counterstaining with DAPI (1 μg/ml) for 10 min. To visualize the fluorochromes confocal microscopy was applied (LSM 780, Carl Zeiss).

Osteogenic differentiation via biochemical cues

To induce osteogenic differentiation, ITSCs were cultivated in DMEM containing 10% fetal calf serum (FCS, Sigma-Aldrich) at a density of 3×10^3 /cm^2 for 48 h followed by cultivation in an osteogenic induction medium containing 100 nM dexamethasone (Sigma-Aldrich), 10 mM β-glycerophosphate (Sigma-Aldrich) and 0.05 mM L-ascorbic acid-2-phosphate (Sigma-Aldrich) at 37 °C and 5% CO_2 in a humidified incubator (Binder). ALP activity was measured 7 days after induction (DAI) using the Alkaline Phosphatase Detection Kit (Millipore) according to the manufacturer's guidelines. Biological mineralization was visualized with Von Kossa and Alizarin Red S staining 21 days after induction. For the detection of the staining AMG EVOS xl microscope (PeqLab Biotechnology) was used.

Osteogenic differentiation via topological cues

To topologically induce osteogenic differentiation, ITSCs were plated in α-MEM containing 10% fetal calf serum on a flat titanium surface, a titanium surface with anisotropically arranged 30 nm pores and an anisotropic configuration of 100 nm pores (see Fig. 2A) at a density of 10^4/cm^2 without additional (biochemical) osteogenic cues. As a positive control, ITSCs on the flat titanium surface were treated with the osteogenic induction medium (see above). Cells were further cultivated at 37 °C and 5% CO_2 in a humidified incubator (Binder).

Detection of calcium deposition (Alizarin red S and Von Kossa staining)

ITSCs differentiated for 21 days were fixed for 15 min using 4% PFA followed by wash steps using PBS (1×) for Alizarin Red S staining or with ddH_2O for Von Kossa staining. For Alizarin Red S staining, the staining solution (1% Alizarin Red in ddH_2O, Waldeck, Münster, Germany) with a pH value of 4.3 was applied for 5 min at RT followed by imaging using the AMG EVOS xl microscope (PeqLab Biotechnology). For Von Kossa staining, ddH_2O containing 5% silver nitrate (Fluka Chemie, Buchs) was applied for 60 min under UV light followed by washing with ddH_2O. Afterwards, ITSCs were incubated in 5% sodium thiosulphate solution (in ddH_2O, Fluka Chemie) for 3 min and washed using ddH_2O. Kernechtrot-solution containing 100 ml ddH_2O, 5 g aluminium sulphate and 0.1% Kernechtrot (Merck) was applied for 5 min followed by washing with 100% ethanol and two times with 96% ethanol. Imaging was performed as described for Alizarin Red Staining. For simultaneous detection of nuclei and Alizarin S staining, confocal laser scanning microscopy was applied (LSM780, Carl Zeiss).

Calcium assay (Alizarin Red S dye recovery)

To quantify the amount of deposited calcium, the different test substrates were immersed in 400 μl 10% acetic acid and incubated under shaking for 30 min at RT. After the monolayer was detached, the solution was heated to 85 °C for 10 min. Subsequently the samples were centrifuged at 20 000 ×*g* for 15 min and the supernatant was transferred to a new test tube. Prior to photometry, the pH value was set to 4.3 and the optical density was measured at a wavelength of 405 nm using an Ultraspec 2100 pro photometer (Amersham Bioscience). Alizarin Red S content (dye recovery) of the solution was determined using a standard curve.

RNA isolation, primer design and qRT-PCR

Total RNA-isolation from osteogenically differentiated and control-ITSCs was harvested at days 0, 7, 12 and 21 and the cDNA was synthesized as described in Martin et al. (2012). Quantitative RT-PCR for Integrin β1, Integrin α2, Bmp2, Osterix, Runx2 and Osteocalcin was performed as triplicate applying Platinum SYBR Green, qPCR SuperMix-UDG (Invitrogen, Life Technologies GmbH) and Rotor Gene 6000 (QIAGEN).

Primer sequences are as indicated in Table 1. GAPDH was used as a housekeeping gene control.

Scanning electron microscopy

To examine the used porous substrates the titanium covered discs were imaged using a scanning electron microscope (SEM, FEI Helios Nanolab 600) in secondary electron mode. The pore density was determined by averaging the pore densities measured on 14 randomly chosen ROIs with a size of 6.25 μm^2 each. For high resolution electron microscopy cells were cultured on the two porous test substrates for 3 days. The cells were primarily fixed by aldehydes, post-fixed in 1.5% OsO_4, shock frozen in hydrated state in liquefied propane at $-185\ ^\circ C$ and subsequently freeze-dried at 10^{-5} mBar. Uncoated specimens were examined in an SEM as mentioned above.

Proliferations and viability assay

To characterize the biocompatibility of the used polycarbonate membranes, proliferation and viability assays were performed. ITSCs were seeded and cultivated as described above on flat titanium, 30 nm pores and 100 nm pores. After 1 d, 2 d, 3 d and 4 d of cultivation, cells were fixed with PFA and subsequently stained with DAPI as described in 'Immunocytochemistry and staining for F-actin'. To determine the proliferation, cell density on the respective substrate was calculated by counting the amount of cell nuclei on seven independent ROIs with a size of 1 mm^2 for each time point and substrate. To ascertain the viability, ITSCs were cultured for 3 d, stained using DAPI followed by counting of total vs. apoptotic nuclei.

Statistical analysis

All experiments were performed at least as triplicate. Statistical significance was determined by ANOVA with Bonferroni correction, using GraphPad's Prism Software. p values <0.05 were considered significant.

Table 1 Table of used primers for PCR.

Primer	Sequence (5′–3′)
Bmp 2 fwd	AGACCTGTATCGCAGGCACT
Bmp 2 rev	AAACTCCTCCGTGGGGATAG
Osterix fwd	GCTTATCCAGCCCCCTTTAC
Osterix rev	CACTGGGCAGACAGTCAGAA
Integrin α2 fwd	GTCCTTGGATGGCTATGGAG
Integrin α2 rev	TTGCACTGAAGCAGAGTTTGA
Integrin β1 fwd	AAGTTTCAAGGGCAAACGTG
Integrin β1 rev	GGGGTAATTTGTCCCGACTT
Osteocalcin fwd	CCTTTGTGTCCAAGCAGGAG
Osteocalcin rev	TCAGCCAACTCGTCACAGTC
Gapdh fwd	CTGCACCACCAACTGCTTAG
Gapdh rev	GTCTTCTGGGTGGCAGTGAT

Results

Human neural crest-derived ITSCs form neurospheres and express stem cell marker nestin

ITSCs isolated and cultivated from inferior turbinate of the nasal cavity (see scheme in Fig. 1A) were able to form neurospheres, if cultivated under serum-free conditions in the presence of EGF and FGF-2 (Fig. 1B). Immunocytochemical staining of ITSC-derived neurospheres for the neural- and neural crest stem cell marker nestin revealed its expression in majority of the cells (Fig. 1C).

Cultivated ITSCs are able to differentiate into osteogenic lineage after cultivation in the presence of biochemical osteoinductive cues

Cultivation of ITSCs in an osteogenic induction medium containing dexamethasone, β-glycerophosphate and L-ascorbic acid-2-phosphate led to osteogenic differentiation within 7 days visualized by strong ALP activity (Fig. 1D, left). Additionally, a late marker of osteoblastic differentiation, the mineralization was investigated after 21 days of culture in an osteogenic induction medium. Mineralization was visualized by Alizarin Red S and Von Kossa staining confirming Ca^{2+} deposition within differentiated cells (Fig. 1D, middle and right).

Characterization of the nanoporous titanium surface

In order to characterize the nanoporous titanium surfaces on polycarbonate membranes scanning electron microscopy was used. Micrographs of titanium surfaces clearly revealed a uniform titanium coating as well as anisotropic arrangement and a homogenous pore size of 30 nm or 100 nm, respectively (Fig. 2A). According to the manufacturer's information, the pore density is in the same order of magnitude for both pore sizes (30 nm and 100 nm) with slight variations caused by the manufacturing procedure ($4–6 \times 10^8$ pores/cm^2). Prior to the experiments the pore number was confirmed using SEM revealing a density of $5.82 \pm 0.93/\mu m^2$ (30 nm pores) and $3.0 \pm 0.74/\mu m^2$ (100 nm pores) respectively. High magnification SEM-micrographs of ITSC cultivated for three days on 30 nm pores (Fig. 2B, left; arrows) revealed a clear direct interaction of cellular protrusions with the pores manifested as membrane tethers. In contrast, cells cultivated on 100 nm pores grew over the pores without obvious signs of tethering (Fig. 2B, right, arrowheads).

Nanoporous titanium surface is biocompatible

In order to investigate the biocompatibility of nanoporous titanium surfaces with different sizes, ITSCs were cultivated on the respective substrate for three days followed by fixation and analysis using SEM. Micrographs of ITSCs clearly revealed the biocompatibility of the titanium surface with 30 nm and 100 nm pore size as demonstrated by typical morphology of viable, non-apoptotic cells (supplementary Fig. 1). Cultivation on 30 nm pores resulted in rather spindle-like morphology (supplementary Fig. 1, left image) in contrast to ITSCs cultivated on 100 nm pores, which were generally round (supplementary Fig. 1, right image). ITSCs cultivated for four

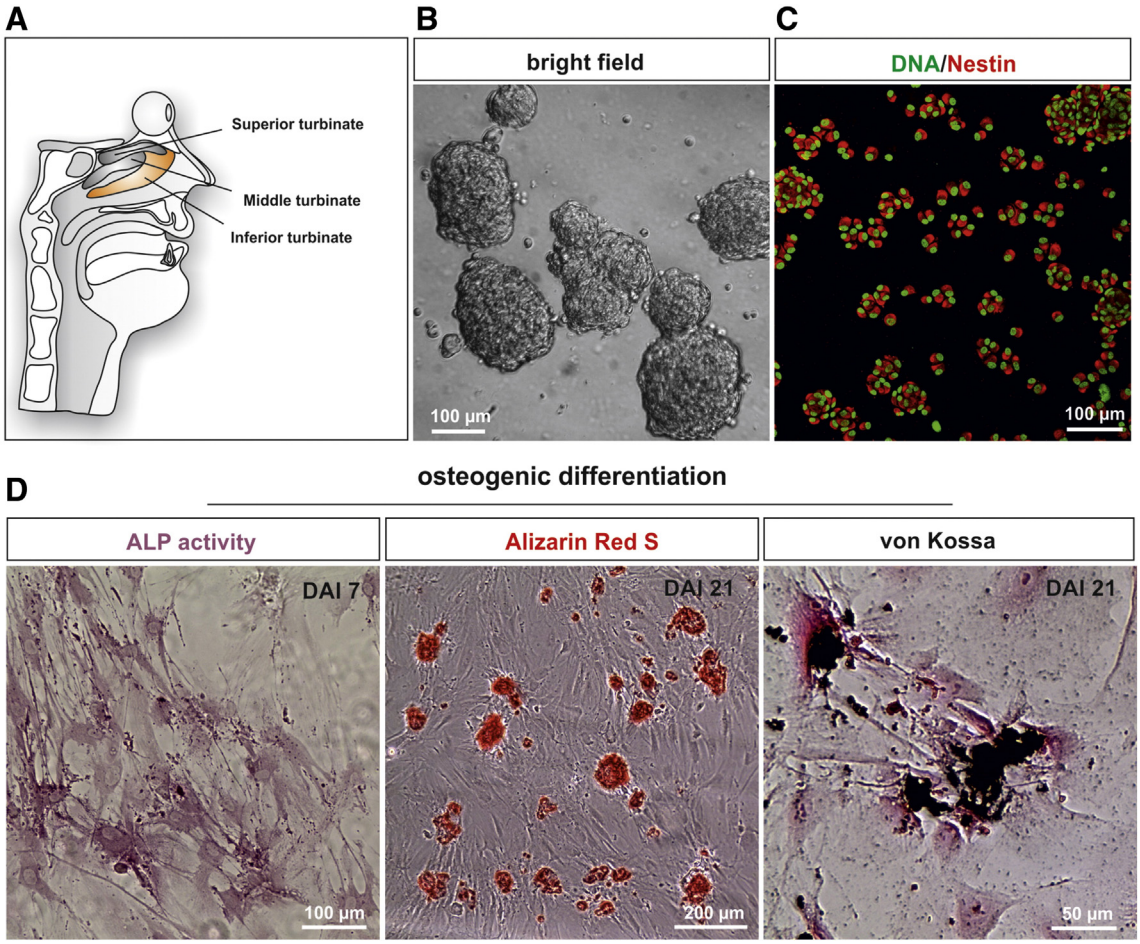

Figure 1 Endogenous niche, characterization and osteogenic differentiation of neural crest-derived inferior turbinate stem cells. A. Schematic illustration of human nasal cavity containing the superior, middle and inferior turbinate. B. Neural crest-derived stem cells can be isolated from the inferior turbinate and cultivated under serum-free conditions in the presence of FGF-2 and EGF leading to formation of self-adherent neurospheres. C. Cultivated inferior turbinate stem cells express the neural crest stem cell marker nestin as visualized by immunocytochemical staining. Scale bar: 100 μm. D. Osteogenic differentiation potential of isolated neural crest-derived inferior turbinate stem cells. Cells differentiated in osteogenic lineage using biochemical cues revealed high ALP activity (left image, days after induction 7 (DAI 7), scale bar: 100 μm) and mineralization visualized by Alizarin Red S (middle image, DAI 21, scale bar: 200 μm) and von Kossa staining (right image, DAI 21, scale bar: 50 μm). DAI: days after induction.

days (96 h) on a flat titanium substrate and 30 nm pores showed proliferative behavior typical for ITSCs with low percentage of apoptotic cells (Fig. 3D–E). Remarkably, although the majority of ITSCs cultivated on 100 nm pores survived, increased apoptosis and reduced proliferation were detected. (Fig. 3D–E).

Cultivation of ITSCs on a titanium surface with 30 nm pore size results in osteogenic differentiation without additional biochemical cues

To investigate the influence of nanotopology of the titanium surface on differentiation of ITSCs, cells were cultivated on flat titanium and nanoporous titanium surfaces (30 nm and 100 nm pore size) free of biochemical osteoinductive cues. As a positive control, an osteoinductive medium containing dexamethasone, β-glycerophosphate and L-ascorbic acid-2-phosphate was applied on cells cultured on flat titanium. Seven days after induction (DAI 7), cells were assayed for activity of alkaline phosphatase (ALP, Fig. 3A, upper panel). No ALP-activity was observed in ITSCs cultivated on a flat Ti-surface and on 100 nm pores. In contrast, biochemically induced cells and ITSCs cultivated on 30 nm pores revealed a clear ALP signal. In order to further investigate the osteogenic differentiation, Ca^{2+} deposition was visualized by Alizarin Red S and von Kossa staining after 21 days of cultivation (DAI 21) on respective surface or in the presence of an osteogenic induction medium. Distinct mineralization was observed in ITSCs differentiated via biochemical cues and cultivated on 30 pores (Fig. 3A, middle row and lower row). In contrast, no signs of mineralization were observed in cells cultivated on a flat Ti surface and on nanoporous titanium with 100 nm pores. In order to prove the Ca^{2+} deposition by ITSCs, differentiated ITSCs on a 30 nm pore surface were counterstained for DNA using DAPI followed by confocal laser scanning microscopy (Fig. 3B). This approach clearly revealed the presence of nuclei in close proximity to the Alizarin Red S signal. Mineralization was quantified using standard Alizarin Red S dye recovery assay, which is commonly used for quantitative investigation of osteogenic

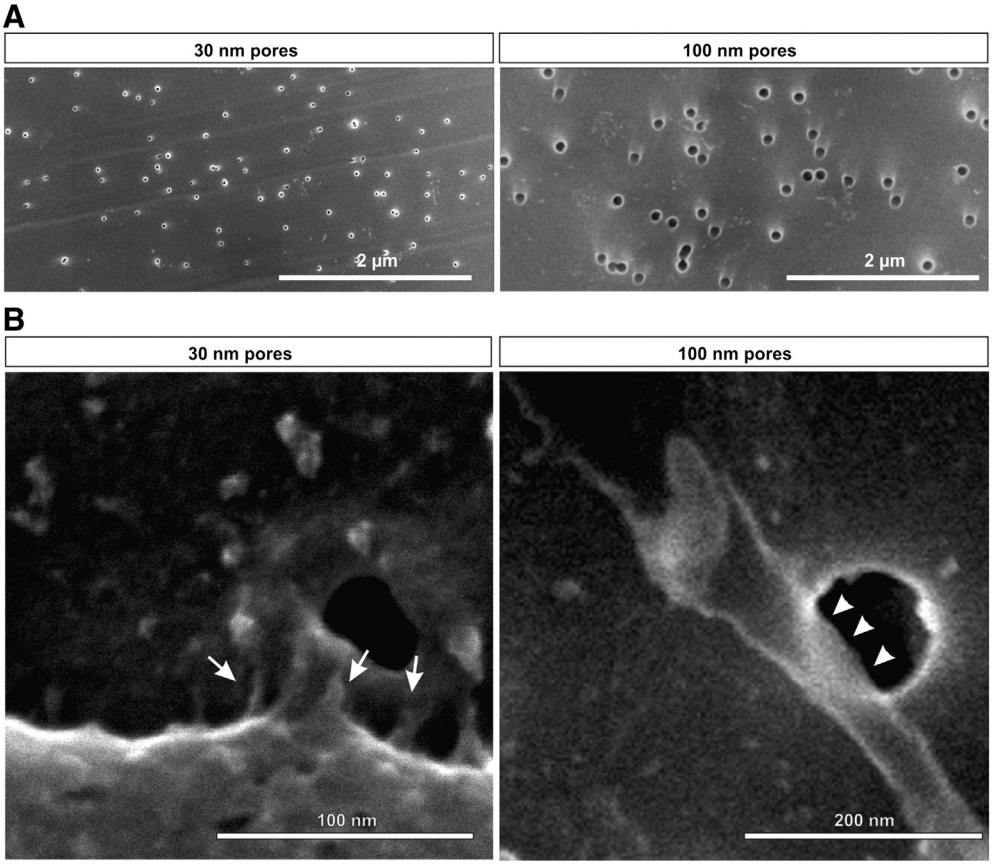

Figure 2 Characterization of nanoporous titanium surfaces and interaction of neural crest-derived stem cells with pores of different sizes. A. Scanning electron microscopy was applied to characterize the nanoporous titanium surfaces on polycarbonate membranes. Micrographs of titanium surfaces reveal uniform titanium coating and anisotropic arrangement of pores (30 nm or 100 nm). B. Neural crest-derived human inferior turbinate stem cells were cultivated on nanoporous titanium substrates for three days followed by analysis using scanning electron microscopy. High magnification micrographs revealed a clear direct interaction of cellular protrusions with the 30 nm pores manifested as membrane tethers (arrows). Cells cultivated on 100 nm pores grew over the pores without obvious signs of tethering (arrowheads).

differentiation of MSCs (Gregory et al., 2004). For ITSCs cultivated on flat Ti and 100 nm pores no dye recovery was measured, whereas cells differentiated via biochemical cues and by cultivation on 30 nm pores revealed comparable Alizarin Red S recovery values (~55 nmol for 30 nm pores and ~72 nm for biochemical induction, Fig. 3C).

ITSCs differentiated on a 30 nm pore surface up-regulate osteogenesis-related transcripts

To test the influence of the surface on the quantity of pro-osteogenic transcripts, ITSCs were cultivated on respective substrate followed by RNA-isolation and quantitative RT-PCR. At DAI 7, a significant increase of Bmp2 was observed in the 30 nm approach, compared to cell cultivated on flat Ti and on 100 nm pores (Fig. 4A). Moreover, cultivation on 30 nm pores resulted in highly elevated expression of Osteocalcin (DAI 12) and Osterix (DAI 21), which were not detected after cultivation on flat Ti and 100 nm pores (Fig. 4A). In a further assay, the timeline of induction of Osterix and Osteocalcin in ITSCs cultivated on 30 nm pores was investigated (Fig. 4B). Osterix-induction was detected at DAI 21, whereas Osteocalcin was elevated at DAI 12 and further increased at DAI 21 (Fig. 4B).

Cultivation of ITSCs on the Ti surface equipped with 30 nm pores elevates expression of Integrin subunits β1 and α2

Since the Integrin subunits β1 and α2 are known to induce the expression of Osteocalcin and increased alkaline phosphatase activity in osteogenic precursor cells and MSCs due to topographical cues (Olivares-Navarrete et al., 2008; Wang et al., 2006), we tested their potential induction in ITSCs after cultivation on 30 nm pores using qRT-PCR (Fig. 5A). Integrin β1 subunit was up-regulated on the first day of cultivation and remained to be expressed at a significantly higher level compared to the flat titanium substrate. In contrast, the Integrin α2 subunit displayed a later but still significant up-regulation when ITSCs were cultivated on a 30 nm pore surface for 7 days (Fig. 5A).

Cultivation of ITSCs on 30 nm pores leads to increased phosphorylation of FAK at Y397

Due to the crucial role of FAK-phosphorylation at Y397 in early osteogenic differentiation acting as a link between Integrin–substrate binding and the downstream signaling (Salasznyk et al., 2007), immunocytochemical stainings against phosphorylated FAK at its autophosphorylation site Y397 with subsequent visualization via confocal laser scanning microscopy were applied. Here, a highly increased level of FAK-phosphorylation was observed in ITSCs cultivated on 30 pores for 24 h, compared to the flat Ti approach (Fig. 5B).

ITSCs cultivated on flat Ti form diffuse actin fibers with weak polarity in contrast to well-defined polarized F-actin fibers in ITSCs on a 30 nm pore titanium substrate

Increased FAK phosphorylation in cells osteogenically differentiated onTi surfaces is known to be accompanied by

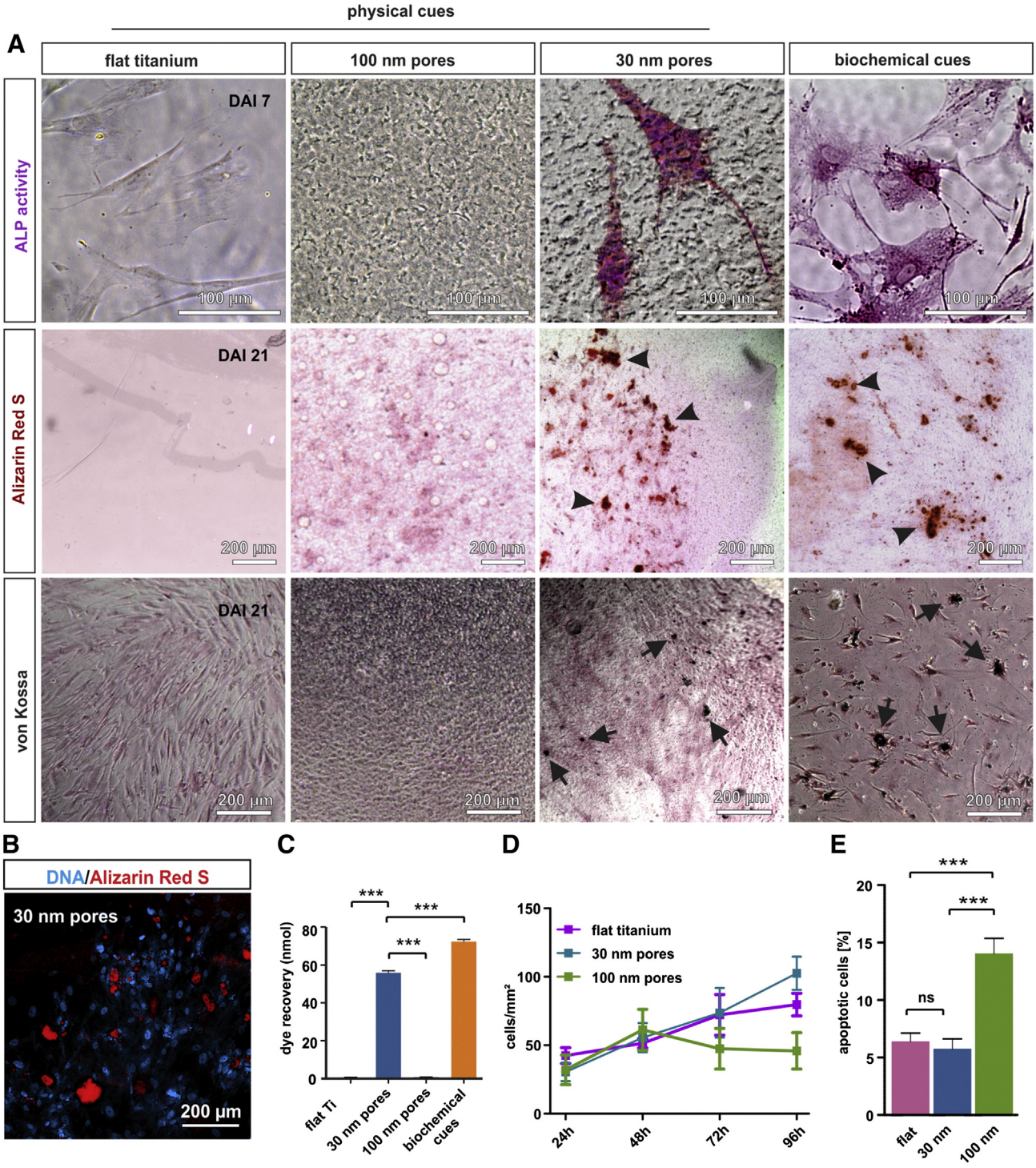

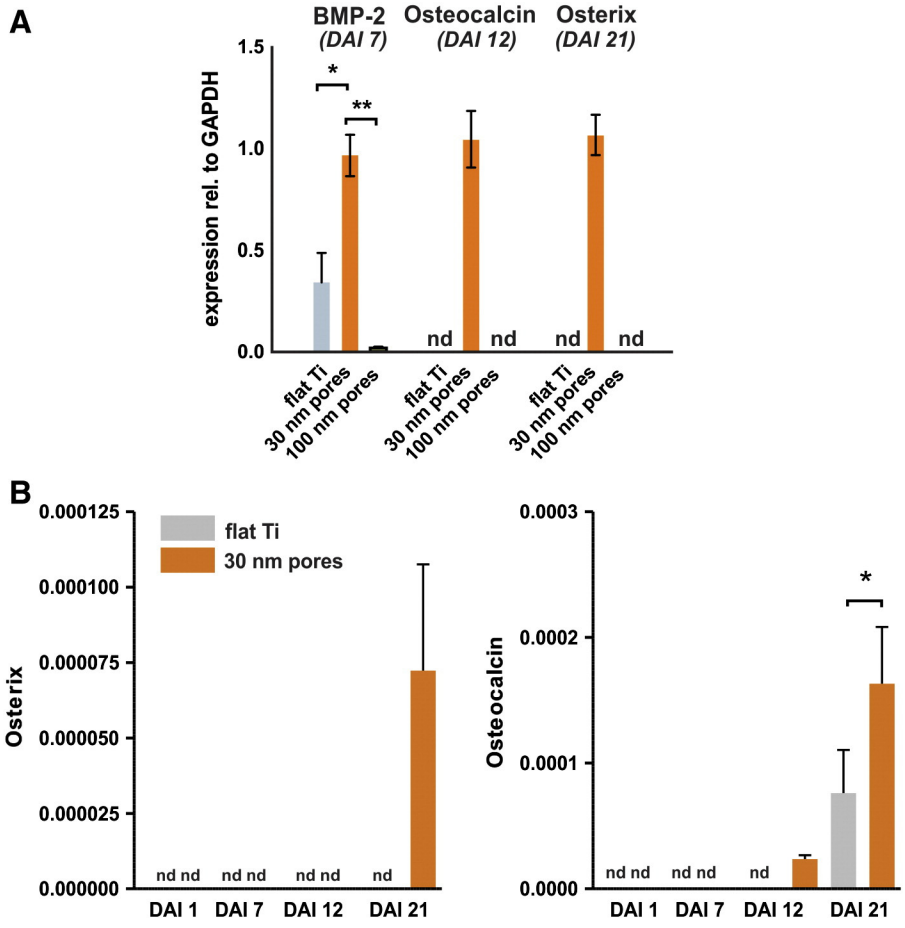

Figure 4 Osteogenic induction by nanotopological cues (30 nm pores) results in up-regulation of osteogenesis-related transcripts. A. Cells were cultivated on respective substrate followed by quantitative RT-PCR. At DAI 7, a significant increase of Bmp2 was observed in the 30 nm-approach in comparison to cells cultivated on flat Ti and 100 nm pores. In addition, cultivation on 30 nm pores increases expression of Osteocalcin (DAI 12) and Osterix (DAI 21). B. Timeline of induction of Osterix and Osteocalcin. Up-regulation of Osterix was detected at DAI 21, whereas Osteocalcin was induced already at DAI 12. Error bars: SEM, $^{**}P < 0.01$, $^{*}P < 0.05$.

dramatic re-arrangement of the actin (Okumura et al., 2001). Therefore, ITSCs on flat Ti and on Ti surface owning 30 nm pores were fixed after 24 h of cultivation and stained for F-actin using Rhodamine-coupled phalloidin. Analysis via confocal laser scanning microscopy revealed highly ordered, polarized actin fibers in ITSCs on 30 nm pores, whereas cells cultivated on the flat Ti surface demonstrated diffusely ordered F-actin (Fig. 5C).

Figure 3 Nanoporous titanium substrate with a pore size of 30 nm induces osteogenic differentiation without negative effects on proliferation and apoptosis of ITSCs. A. Cells were cultivated on flat titanium and nanoporous titanium surfaces (30 nm and 100 nm pore size) and in the presence of biochemical osteoinductive cues. Seven days after induction (DAI 7), cells were assayed for activity of alkaline phosphatase. ALP-activity was observed only in cells cultivated on 30 nm pores and after biochemical induction. Ca^{2+} deposition was visualized after 21 days of cultivation using Alizarin Red S and von Kossa staining. Alizarin Red S (arrowheads) and von Kossa signals (arrows) were observed on cells differentiated via biochemical cues and on 30 pores, whereas no signs of mineralization were observed on cells cultivated on a flat Ti surface and on nanoporous titanium with 100 nm pores. B. Alizarin Red S stained Ca^{2+} -depositions are generated by living cells. Differentiated stem cells on a 30 nm pore surface were counterstained for DNA using DAPI. Confocal laser scanning microscopy clearly revealed the presence of nuclei in close proximity to the Alizarin Red S signal. C. Quantification of mineralization was performed using Alizarin Red S dye recovery assay. For inferior turbinate stem cells cultivated on flat Ti and 100 nm pores no dye recovery was measured, whereas cells differentiated via biochemical cues and by cultivation on 30 nm pores demonstrated comparable Alizarin Red S recovery values. Error bars: SEM, $^{***}P < 0.0001$. D–E. ITSCs were seeded and cultivated as described above on flat titanium, 30 nm pores and 100 nm pores. Cultivation on 30 nm pores and on flat titanium supported proliferation of ITSCs, whereas cultivation on 100 nm pores led to reduced proliferative behavior and increased apoptosis. To ascertain the viability, ITSCs were cultured for 3 d, stained using DAPI followed by counting of total vs. apoptotic nuclei. Error bars: SEM, $^{***}P < 0.0001$.

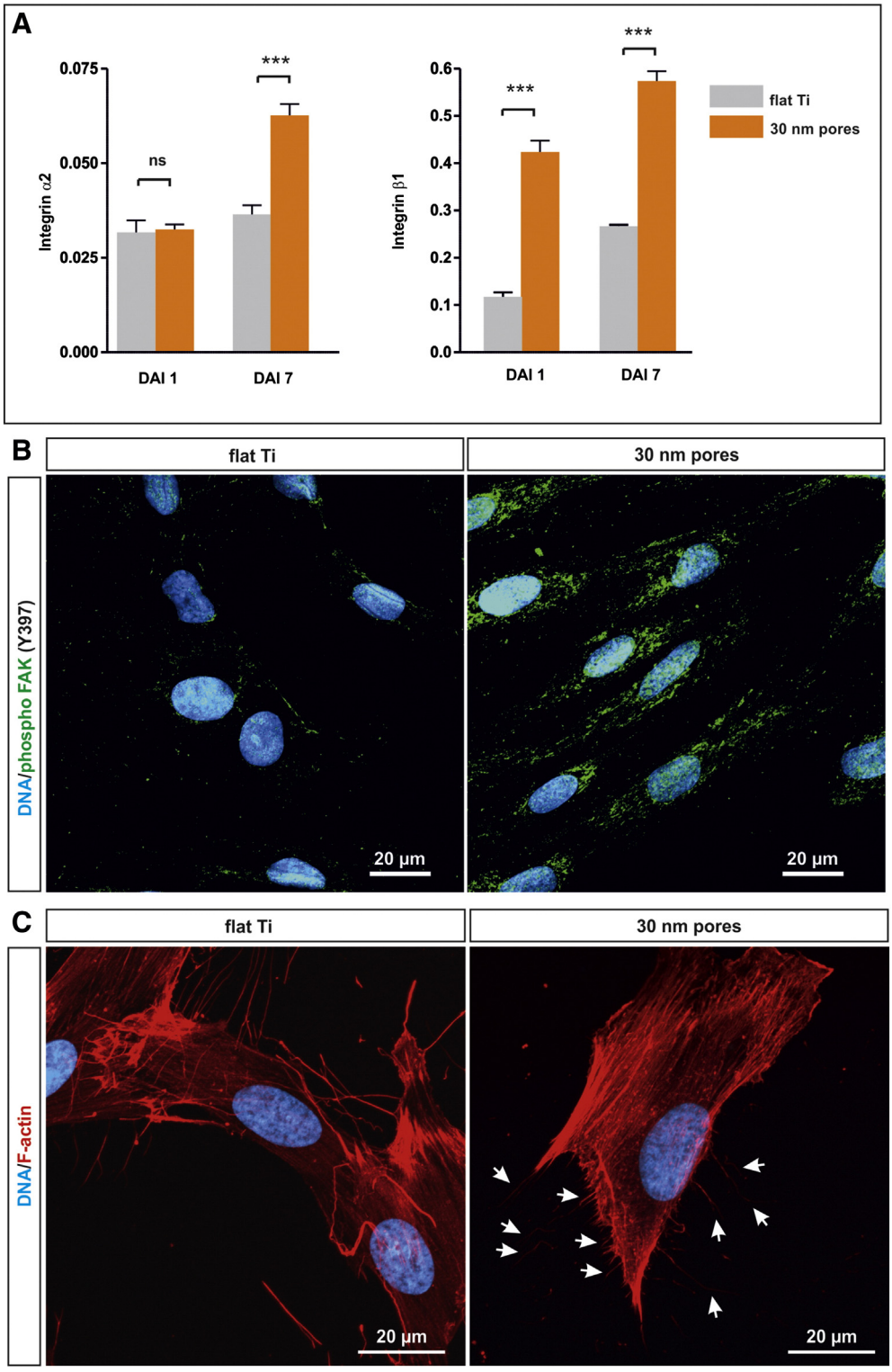

Figure 5 Osteogenically differentiated inferior turbinate stem cells up-regulate Integrin subunits α2 and β1, increase the phosphorylation of FAK at Y397 and reveal dramatic re-arrangement of the actin cytoskeleton. A. Inferior turbinate stem cells were cultivated on 30 nm pores or flat Ti for up to seven days followed by qRT-PCR. Up-regulation of the transcript for Integrin β1 was detected on the first day of cultivation and remained at a significantly higher level in the 30 nm approach compared to the flat titanium substrate. The Integrin α2 subunit displayed significant up-regulation on a 30 nm pore surface after 7 days of cultivation. Error bars: SEM, ***$P < 0.0001$. B. Cells cultivated on respective substrate for 24 h were immunocytochemically stained against phosphorylated FAK (Y397) with subsequent confocal laser scanning microscopy. Highly increased level of FAK-phosphorylation was observed in ITSCs cultivated on 30 pores in comparison to the flat Ti approach. C. Stem cells cultivated for 24 h on flat Ti and on Ti surface owning 30 nm pores stained for F-actin using Rhodamine-coupled phalloidin. Analysis via confocal laser scanning microscopy revealed highly ordered actin fibers in the 30 nm approach (arrows), whereas cells cultivated on a flat Ti surface demonstrated diffusely ordered F-actin.

Discussion

Adult cranial neural crest-derived stem cells are of extraordinary plasticity and can give rise to ectodermal cell types (e.g., peripheral sensory and autonomic neurons, glial cells and pigment cells), as well as to mesenchymal cell types (e.g., perivascular muscle cells, bones and connective tissues) (reviewed in (Kaltschmidt et al., 2012).

Besides the differentiation into ectodermal derivatives, cranial NCSCs contribute efficiently to craniofacial bone formation during normal development and after experimental transplantation. Importantly, bones formed by transplanted NCSCs are distinct from bone structures generated by mesenchymal stem cells and resemble the endogenous tissue more closely (Chung et al., 2009).

This intrinsic feature and their easy accessibility make cranial NCSCs promising candidates for use in regenerative medicine either alone, or combined with materials which may improve the graft adherence and/or influence their differentiation into the desired fate. In this context, autologous stem cells could be pre-cultivated on prostheses, potentially influencing their integration into patient's tissue. In this context, titanium is a highly promising material, since it is generally biocompatible and has mechanical properties similar to bone. It has been reported that nanoscale topology of different substrates including titanium is able to induce osteogenic differentiation in different mammalian cell types including osteogenic progenitors, osteoblast cell lines and human mesenchymal stem cells (Dalby et al., 2006; Lavenus et al., 2010, 2011; Wennerberg and Albrektsson, 2009). However, to our knowledge, there are no reports on osteogenic differentiation of neural crest-derived human cells induced solely by topology of the substrate.

In this study, we show for the first time, that a nanoporous titanium surface with a pore diameter of 30 nm is able to induce osteogenic differentiation of adult human neural crest-derived stem cells free of biochemical cues such as dexamethasone. We demonstrate that the titanium surface is biocompatible with neural crest-derived ITSCs and that an anisotropic arrangement of pores with a diameter of 30 nm is able to induce osteogenic differentiation of this cell type. In contrast, although allowing survival of ITSCs, pores with a diameter of 100 nm had no osteoinductive effects (Fig. 3). These finding are in general accordance with a study by Lavenus et al. (2011) showing that a 30 nm pore size is osteoinductive for human MSCs. Remarkably, we measured high levels of OCN-transcript on 30 nm pores, whereas no expression was observed on a flat titanium substrate and on 100 nm pores. Interestingly, in their study, Lavenus et al. demonstrated high OCN-levels on 300 nm and not on 30 nm. However, no Alizarin Red S signal was observed on 300 nm suggesting incomplete differentiation. Moreover, Alizarin signal was observed after differentiation of 150 nm pores. Since the detection of Alizarin Red S bears the risk of overestimation due to false-positive signal caused by cell debris, we applied a more stringent test by additional detection of intact nuclei revealing specific signals exclusively on 30 nm pores and after osteogenic differentiation by biochemical cues (Fig. 3B–C).

In a further approach Park et al. were able to show that cultivation of MSCs on vertically oriented TiO_2 nanotubes with lateral spacing of 15–30 nm for 4 days followed by biochemical induction leads to increased FAK phosphorylation, mineralization and up-regulation of OCN, which is in general accordance with our study (Park et al., 2007). Importantly, spacing of 100 nm was not osteoinductive and led to strong induction of apoptosis. Remarkably, due to the use of biochemical cues after five days of cultivation, it cannot be excluded that the effects observed by Park et al. were at least partly induced by dexamethasone and other components of the medium instead of the topology of the material. In 2009, Oh et al. reported that cultivation of MSCs on TiO_2 nanotubes with a diameter of 100 nm results in up-regulation of osteogenic markers, whereas 30 nm nanotubes have no osteoinductive effects (Oh et al., 2009). In our study, cultivation of human stem cells on 100 nm pores led to increased apoptosis (Fig. 3E) and had no osteoinductive effects. We further demonstrate that ITSCs directly interact with 30 nm pores in terms of tethering, whereas cells cultivated on 100 nm pores showed no signs of such direct interaction (Fig. 2B): Moreover, using qRT-PCR, we observed induction of transcripts associated with osteogenic differentiation, including Bmp2, Osterix and Osteocalcin (Fig. 4). Bmp2 is known to induce the expression of Osterix (Lee et al., 2003) which in turn initiates terminal differentiation of osteoblasts and elevates the expression of Osteocalcin (Niger et al., 2011). Noteworthy, Osteocalcin is secreted uniquely by osteoblastic cells and stimulates the generation of calcium deposits (Lian et al., 1998). This corresponds with distinct Ca^{2+}-deposition visualized by Alizarin Red S and von Kossa staining after 21 days of cultivation (DAI 21) on a 30 nm titanium surface, but not on flat Ti or titanium surface with 100 nm pores (Fig. 3). Due to the prominent role of the Integrin subunits $\alpha 2$ and $\beta 1$ in early osteogenic differentiation and induction of Osteocalcin (Olivares-Navarrete et al., 2008; Wang et al., 2006), we investigated their potential up-regulation after cultivation on the nanoporous titanium surface owning 30 nm pores. Here, we demonstrated significant induction of both subunits compared to cell cultivated on a flat Ti surface (Fig. 5A). Importantly, these results correspond to dramatically increased FAK phosphorylation at Y397 after topological induction of osteogenic differentiation. Remarkably, besides its pivotal role in cell spreading and migration (Jacamo et al., 2007), FAK-phosphorylation at Y397 plays a crucial role in early osteogenic differentiation due to topological cues providing a link between Integrin–substrate binding and the downstream signaling (Salasznyk et al., 2007).

Already in 2001 Okumura et al. reported that increased FAK phosphorylation on Ti surfaces during osteogenic differentiation is directly linked to re-arrangement of the actin cytoskeleton (Okumura et al., 2001). In order to investigate potential differences in actin cytoskeleton architecture between ITSCs cultivated on nanoporous Ti substrate (30 nm pores) and on flat Ti, we stained F-actin using Rhodamine-coupled phalloidin. In our approach we observed highly ordered, polarized cytoskeletal fibers in ITSCs on 30 nm pores, which is consistent with re-arrangement of cytoskeleton during osteogenic differentiation (reviewed in (Chen and Jacobs, 2013)).

Conclusions

In sum, we were able to show that cultivation of human neural crest-derived ITSCs on a nanoporous titanium surface

with an anisotropic arrangement of 30 nm pores leads to osteogenic differentiation without the need of additional biochemical cues. This nanotopologically induced osteogenic differentiation is accompanied by up-regulation of Integrin subunits $\alpha 2$ and $\beta 1$, Bmp2, Osterix and Osteocalcin. In addition, we demonstrated high activity of alkaline phosphatase, increased phosphorylation of FAK at Y397, re-arrangement of actin cytoskeleton and finally significantly elevated Ca^{2+} deposition by differentiated cells (summarized in Fig. 6). In the future, this approach could be used to improve the integration of prostheses via populating with autologous, osteogenically pre-differentiated neural crest-derived cells.

Supplementary data to this article can be found online at http://dx.doi.org/10.1016/j.scr.2014.04.017.

Acknowledgments

The excellent technical help of Angela Krahlemann-Köhler is gratefully acknowledged. This study was supported by the University of Bielefeld and by a Grant of the German Ministry of Research and Education to BK (BMBF, Grant: 01GN1006A). The authors acknowledge the support for the Article Processing Charge by the Deutsche Forschungsgemeinschaft (DFG) and the Open Access Publication Funds of Bielefeld

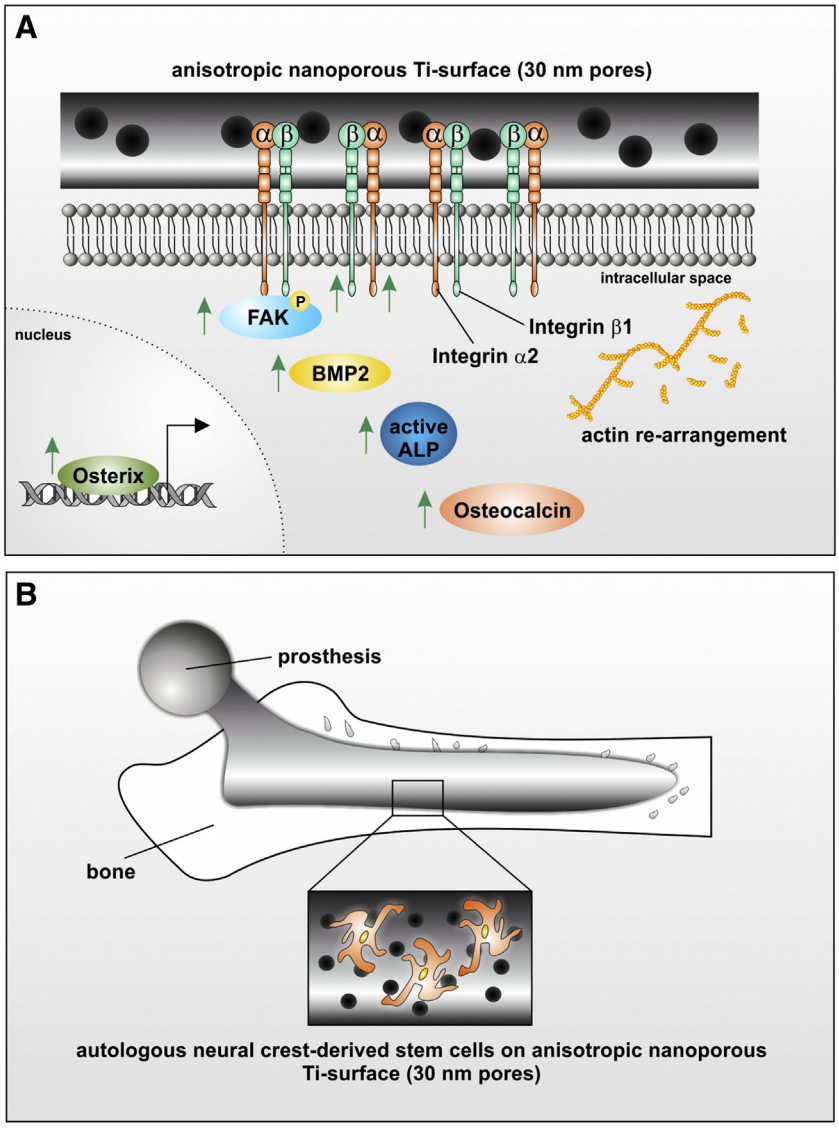

Figure 6 A. Schematic representation of cellular events induced by cultivation of neural crest-derived inferior turbinate stem cells on anisotropically arranged 30 nm pores on the titanium surface. Osteogenic differentiation induced by nanotopology of the titanium surface leads to up-regulation of Integrin subunits $\alpha 2$ and $\beta 1$, Bmp2, Osterix and Osteocalcin. Moreover, high activity of alkaline phosphatase, increased phosphorylation of FAK at Y397 and re-arrangement of actin cytoskeleton can be observed. B. Potential clinical use of a nanoporous titanium surface in combination with autologous neural crest-derived cell for improved integration of prostheses and bone regeneration. Human neural crest-derived stem cells may be isolated from the given patient prior their cultivation on nanoporous titanium prostheses potentially leading to enhanced graft adherence, better integration of the prosthesis and finally improved clinical outcome.

University Library. We thank Holger Sudhoff for providing human inferior turbinates.

References

Arnold, W.H., Becher, S., Dannan, A., Widera, D., Dittmar, T., Jacob, M., ..., Grimm, W.D., 2010. Morphological characterization of periodontium-derived human stem cells. Ann. Anat. 192 (4), 215–219. http://dx.doi.org/10.1016/j.aanat.2010.05.004.

Baek, W.Y., Kim, Y.J., de Crombrugghe, B., Kim, J.E., 2013. Osterix is required for cranial neural crest-derived craniofacial bone formation. [Research Support, Non-U.S. Gov't]. Biochem. Biophys. Res. Commun. 432 (1), 188–192. http://dx.doi.org/10.1016/j.bbrc.2012.12.138.

Calloni, G.W., Le Douarin, N.M., Dupin, E., 2009. High frequency of cephalic neural crest cells shows coexistence of neurogenic, melanogenic, and osteogenic differentiation capacities. [Research Support, Non-U.S. Gov't]. Proc. Natl. Acad. Sci. U. S. A. 106 (22), 8947–8952. http://dx.doi.org/10.1073/pnas.0903780106.

Chen, J.C., Jacobs, C.R., 2013. Mechanically induced osteogenic lineage commitment of stem cells. Stem Cell Res. Ther. 4 (5), 107. http://dx.doi.org/10.1186/scrt318.

Chung, I.H., Yamaza, T., Zhao, H., Choung, P.H., Shi, S., Chai, Y., 2009. Stem cell property of postmigratory cranial neural crest cells and their utility in alveolar bone regeneration and tooth development. [Research Support, N.I.H., Extramural]. Stem Cells 27 (4), 866–877. http://dx.doi.org/10.1002/stem.2.

Dalby, M.J., McCloy, D., Robertson, M., Wilkinson, C.D., Oreffo, R.O., 2006. Osteoprogenitor response to defined topographies with nanoscale depths. [Research Support, Non-U.S. Gov't]. Biomaterials 27 (8), 1306–1315. http://dx.doi.org/10.1016/j.biomaterials.2005.08.028.

Dalby, M.J., Gadegaard, N., Curtis, A.S., Oreffo, R.O., 2007. Nanotopographical control of human osteoprogenitor differentiation. [Research Support, Non-U.S. Gov't Review]. Curr. Stem Cell Res. Ther. 2 (2), 129–138.

Dangaria, S.J., Ito, Y., Yin, L., Valdre, G., Luan, X., Diekwisch, T.G., 2011. Apatite microtopographies instruct signaling tapestries for progenitor-driven new attachment of teeth. [Research Support, N.I.H., Extramural]. Tissue Eng. A 17 (3–4), 279–290. http://dx.doi.org/10.1089/ten.TEA.2010.0264.

Delorme, B., Nivet, E., Gaillard, J., Haupl, T., Ringe, J., Deveze, A., ..., Feron, F., 2010. The human nose harbors a niche of olfactory ectomesenchymal stem cells displaying neurogenic and osteogenic properties. Stem Cells Dev. 19 (6), 853–866. http://dx.doi.org/10.1089/scd.2009.0267.

Dong, R., Liu, X., Fan, M., Yang, L., Peng, L., Zhang, L., 2010. Isolation and differentiation of nestin positive cells from rat oral mucosal lamina propria. Differentiation 79 (1), 9–14. http://dx.doi.org/10.1016/j.diff.2009.08.010 (doi: S0301-4681(09)00107-8 [pii]).

Fairbanks, D.N., 1985. Effect of nasal surgery on snoring. South. Med. J. 78 (3), 268–270.

Fink Jr., D.W., 2009. FDA regulation of stem cell-based products. Science 324 (5935), 1662–1663. http://dx.doi.org/10.1126/science.1173712.

Gregory, C.A., Gunn, W.G., Peister, A., Prockop, D.J., 2004. An Alizarin red-based assay of mineralization by adherent cells in culture: comparison with cetylpyridinium chloride extraction. [Comparative Study Research Support, Non-U.S. Gov't Research Support, U.S. Gov't, P.H.S.]. Anal. Biochem. 329 (1), 77–84. http://dx.doi.org/10.1016/j.ab.2004.02.002.

Greiner, J.F., Hauser, S., Widera, D., Muller, J., Qunneis, F., Zander, C., ..., Kaltschmidt, B., 2011. Efficient animal-serum free 3D cultivation method for adult human neural crest-derived stem cell therapeutics. [Research Support, Non-U.S. Gov't]. Eur. Cell. Mater. 22, 403–419.

Greiner, J.F., Grunwald, L.M., Muller, J., Sudhoff, H., Widera, D., Kaltschmidt, C., Kaltschmidt, B., 2014. Culture bag systems for clinical applications of adult human neural crest-derived stem cells. Stem Cell Res. Ther. 5 (2), 34. http://dx.doi.org/10.1186/scrt422.

Hauser, S., Widera, D., Qunneis, F., Muller, J., Zander, C., Greiner, J., ..., Kaltschmidt, B., 2012. Isolation of novel multipotent neural crest-derived stem cells from adult human inferior turbinate. [Research Support, Non-U.S. Gov't]. Stem Cells Dev. 21 (5), 742–756. http://dx.doi.org/10.1089/scd.2011.0419.

Jacamo, R., Jiang, X., Lunn, J.A., Rozengurt, E., 2007. FAK phosphorylation at Ser-843 inhibits Tyr-397 phosphorylation, cell spreading and migration. [Research Support, N.I.H., Extramural]. J. Cell. Physiol. 210 (2), 436–444. http://dx.doi.org/10.1002/jcp.20870.

Kaltschmidt, B., Kaltschmidt, C., Widera, D., 2012. Adult craniofacial stem cells: sources and relation to the neural crest. [Research Support, Non-U.S. Gov't Review]. Stem Cell Rev. 8 (3), 658–671. http://dx.doi.org/10.1007/s12015-011-9340-9.

Kaus, A., Widera, D., Kassmer, S., Peter, J., Zaenker, K., Kaltschmidt, C., Kaltschmidt, B., 2010. Neural stem cells adopt tumorigenic properties by constitutively activated NF-kappaB and subsequent VEGF up-regulation. [Research Support, Non-U.S. Gov't]. Stem Cells Dev. 19 (7), 999–1015. http://dx.doi.org/10.1089/scd.2009.0416.

Kawanabe, N., Murata, S., Murakami, K., Ishihara, Y., Hayano, S., Kurosaka, H., ..., Yamashiro, T., 2010. Isolation of multipotent stem cells in human periodontal ligament using stage-specific embryonic antigen-4. Differentiation 79 (2), 74–83. http://dx.doi.org/10.1016/j.diff.2009.10.005 (doi: S0301-4681(09)00125-X [pii]).

Lavenus, S., Ricquier, J.C., Louarn, G., Layrolle, P., 2010. Cell interaction with nanopatterned surface of implants. [Review]. Nanomedicine (London) 5 (6), 937–947. http://dx.doi.org/10.2217/nnm.10.54.

Lavenus, S., Berreur, M., Trichet, V., Pilet, P., Louarn, G., Layrolle, P., 2011. Adhesion and osteogenic differentiation of human mesenchymal stem cells on titanium nanopores. [Research Support, Non-U.S. Gov't]. Eur. Cell. Mater. 22, 84–96 (discussion 96).

Lee, M.H., Kwon, T.G., Park, H.S., Wozney, J.M., Ryoo, H.M., 2003. BMP-2-induced Osterix expression is mediated by Dlx5 but is independent of Runx2. [Research Support, Non-U.S. Gov't]. Biochem. Biophys. Res. Commun. 309 (3), 689–694.

Lian, J.B., Stein, G.S., Stein, J.L., van Wijnen, A.J., 1998. Osteocalcin gene promoter: unlocking the secrets for regulation of osteoblast growth and differentiation. [Review]. J. Cell. Biochem. Suppl. 30-31, 62–72.

Martin, I., Nguyen, T.D., Krell, V., Greiner, J.F., Muller, J., Hauser, S., ..., Widera, D., 2012. Generation of Schwann cell-derived multipotent neurospheres isolated from intact sciatic nerve. [Research Support, Non-U.S. Gov't]. Stem Cell Rev. 8 (4), 1178–1187. http://dx.doi.org/10.1007/s12015-012-9387-2.

Marynka-Kalmani, K., Treves, S., Yafee, M., Rachima, H., Gafni, Y., Cohen, M.A., Pitaru, S., 2010. The lamina propria of adult human oral mucosa harbors a novel stem cell population. Stem Cells 28 (5), 984–995. http://dx.doi.org/10.1002/stem.425.

Nguyen, T.D., Widera, D., Greiner, J., Muller, J., Martin, I., Slotta, C., ..., Kaltschmidt, B., 2013. Prolonged cultivation of hippocampal neural precursor cells shifts their differentiation potential and selects for aneuploid cells. [Research Support, Non-U.S. Gov't]. Biol. Chem. 394 (12), 1623–1636. http://dx.doi.org/10.1515/hsz-2013-0191.

Niger, C., Lima, F., Yoo, D.J., Gupta, R.R., Buo, A.M., Hebert, C., Stains, J.P., 2011. The transcriptional activity of osterix requires the recruitment of Sp1 to the osteocalcin proximal promoter. [Research Support, N.I.H., Extramural]. Bone 49 (4), 683–692. http://dx.doi.org/10.1016/j.bone.2011.07.027.

Oh, S., Brammer, K.S., Li, Y.S., Teng, D., Engler, A.J., Chien, S., Jin, S., 2009. Stem cell fate dictated solely by altered nanotube dimension. [Research Support, N.I.H., Extramural Research Support, Non-U.S.

Gov't]. Proc. Natl. Acad. Sci. U. S. A. 106 (7), 2130–2135. http://dx.doi.org/10.1073/pnas.0813200106.

Okumura, A., Goto, M., Goto, T., Yoshinari, M., Masuko, S., Katsuki, T., Tanaka, T., 2001. Substrate affects the initial attachment and subsequent behavior of human osteoblastic cells (Saos-2). Biomaterials 22 (16), 2263–2271.

Olivares-Navarrete, R., Raz, P., Zhao, G., Chen, J., Wieland, M., Cochran, D.L., ..., Schwartz, Z., 2008. Integrin alpha2beta1 plays a critical role in osteoblast response to micron-scale surface structure and surface energy of titanium substrates. [Research Support, N.I.H., Extramural Research Support, Non-U.S. Gov't Research Support, U.S. Gov't, Non-P.H.S.]. Proc. Natl. Acad. Sci. U. S. A. 105 (41), 15767–15772. http://dx.doi.org/10.1073/pnas.0805420105.

Park, J., Bauer, S., von der Mark, K., Schmuki, P., 2007. Nanosize and vitality: TiO_2 nanotube diameter directs cell fate. [Research Support, Non-U.S. Gov't]. Nano Lett. 7 (6), 1686–1691. http://dx.doi.org/10.1021/nl070678d.

Salasznyk, R.M., Klees, R.F., Boskey, A., Plopper, G.E., 2007. Activation of FAK is necessary for the osteogenic differentiation of human mesenchymal stem cells on laminin-5. [Research Support, N.I.H., Extramural]. J. Cell. Biochem. 100 (2), 499–514. http://dx.doi.org/10.1002/jcb.21074.

Sjostrom, T., Brydone, A.S., Meek, R.M., Dalby, M.J., Su, B., McNamara, L.E., 2013. Titanium nanofeaturing for enhanced bioactivity of implanted orthopedic and dental devices. [Research Support, Non-U.S. Gov't Review]. Nanomedicine (London) 8 (1), 89–104. http://dx.doi.org/10.2217/nnm.12.177.

Waddington, R.J., Youde, S.J., Lee, C.P., Sloan, A.J., 2009. Isolation of distinct progenitor stem cell populations from dental pulp. Cells Tissues Organs 189 (1–4), 268–274. http://dx.doi.org/10.1159/000151447.

Wang, L., Zhao, G., Olivares-Navarrete, R., Bell, B.F., Wieland, M., Cochran, D.L., ..., Boyan, B.D., 2006. Integrin beta1 silencing in osteoblasts alters substrate-dependent responses to 1,25-dihydroxy vitamin D3. [Research Support, Non-U.S. Gov't Research Support, U.S. Gov't, Non-P.H.S.]. Biomaterials 27 (20), 3716–3725. http://dx.doi.org/10.1016/j.biomaterials.2006.02.022.

Wennerberg, A., Albrektsson, T., 2009. Effects of titanium surface topography on bone integration: a systematic review. [Review]. Clin. Oral Implants Res. 20 (Suppl. 4), 172–184. http://dx.doi.org/10.1111/j.1600-0501.2009.01775.x.

Widera, D., Grimm, W.D., Moebius, J.M., Mikenberg, I., Piechaczek, C., Gassmann, G., ..., Kaltschmidt, B., 2007. Highly efficient neural differentiation of human somatic stem cells, isolated by minimally invasive periodontal surgery. [Research Support, Non-U.S. Gov't]. Stem Cells Dev. 16 (3), 447–460. http://dx.doi.org/10.1089/scd.2006.0068.

Widera, D., Zander, C., Heidbreder, M., Kasperek, Y., Noll, T., Seitz, O., ..., Kaltschmidt, B., 2009. Adult palatum as a novel source of neural crest-related stem cells. Stem Cells 27 (8), 1899–1910. http://dx.doi.org/10.1002/stem.104.